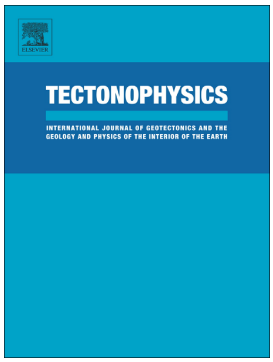

Aseismic creep and gravitational sliding on the lower eastern flank of Mt. Etna: Insights from the 2002 and 2022 fault rupture events between Santa Venerina and Santa Tecla

Giorgio Tringali, Domenico Bella, Franz Livio, Maria Francesca Ferrario, Gianluca Groppelli, Rosario Pettinato, Alessandro Maria Michetti

PII: S0040-1951(23)00127-0

DOI: https://doi.org/10.1016/j.tecto.2023.229829

Reference: TECTO 229829

To appear in: *Tectonophysics*

Received date: 29 October 2022

Revised date: 24 March 2023

Accepted date: 27 March 2023

Please cite this article as: G. Tringali, D. Bella, F. Livio, et al., Aseismic creep and gravitational sliding on the lower eastern flank of Mt. Etna: Insights from the 2002 and 2022 fault rupture events between Santa Venerina and Santa Tecla, *Tectonophysics* (2023), https://doi.org/10.1016/j.tecto.2023.229829

Aseismic creep and gravitational sliding on the lower eastern flank of Mt. Etna: insights from the 2002 and 2022 fault rupture events between Santa Venerina and Santa Tecla

Giorgio Tringali [a]*, Domenico Bella [b], Franz Livio [a], Maria Francesca Ferrario [a], Gianluca Groppelli [c], Rosario Pettinato [b] & Alessandro Maria Michetti [a-d]

Author affiliations:

a) Università degli Studi dell'Insubria, Dipartimento di Scienza ed Alta Tecnologia, Via Valleggio 11, 22100 Como (CO), Italy

b) Studio di Geologia Domenico Bella, Via N. Martoglio 13, 95024 Acireale (CT), Italy

c) CNR – Consiglio Nazionale delle Ricerche, Istituto di Geologia Ambientale e Geoingegneria, Milano (MI), Italy

d) INGV – Istituto Nazionale di Geofisica e Vulcanologia, Osservatorio Vesuviano, via Diocleziano 328, 80124, Napoli (NA), Italy

**Corresponding author:* gtringali@uninsubria.it

Keywords: Etna, aseismic creep, earthquake, surface faulting, volcano-tectonic deformation

Abstract

Fault creep along the lower eastern flank of Mt. Etna volcano has been documented since the end of the 19th century and significantly contributes to the surface faulting hazard in the area. On 29 October 2002, during a seismic swarm related to dyke intrusions, two earthquakes caused extensive damage and surface faulting in an area between the Santa Venerina and Santa Tecla villages. On the same day after the two earthquakes, an episodic aseismic creep occurred along the Scalo Pennisi Fault close to the Santa Tecla coastline. On 8 February 2022, during another aseismic creep event along the Scalo Pennisi Fault, we observed the reopening of the pre-existing 2002 ground ruptures mostly as pure dilational fractures. We mapped the 2002 and 2022 surface ruptures, and collected data on displacement, length, and pattern of ground breaks. Ground ruptures affected structures located along the activated fault segments, including roads, walls and buildings. The 2002 surface faulting propagation can be ascribed to a sliding of the Mt. Etna eastern flank toward the SE, as also suggested by the related shallow seismicity, and InSAR and geodetic data between 2002 and 2005. For the 2022 event, differential InSAR data, acquired in both descending and ascending views, allowed us to decompose Line of Sight (LOS) displacement into horizontal and vertical components. We detect a ~700 long and ~500 m wide deformation zone with a downward and eastward motion (max displacement ~1,5 cm) consistent with a normal fault. We inverted the InSAR–detected surface deformation using a uniform-slip fault model and obtained a shallow detachment for the causative fault, located at ~300 m depth, within the volcanic pile. This is the first in-depth study along the Scalo Pennisi Fault to suggest a shallow faulting that accommodates Mt. Etna E flank gravitational sliding.

1. Introduction

Mt. Etna, one of the most active volcanoes in the world, about 3350 m high, is affected by regional structures and numerous volcano-tectonic features. The eastern and southern flanks of the volcano are affected by surface

faulting along well-known active fault segments (Fig. 1a), due to gravitational collapse of Mt. Etna toward the sea (Groppelli and Tibaldi, 1999; Neri et al., 2007; Solaro et al., 2010; Chiocci et al., 2011; Groppelli and Norini, 2011; Norini and Acocella, 2011; Ruch et al., 2012; Urlaub et l., 2018, 2022). Active faults typically separate shallow sliding blocks within the moving flank (Bonforte et al., 2011; Azzaro et al., 2013). The activity of these faults, that can result in earthquakes (Azzaro, 1999) and aseismic creep events (Rasà et al., 1996), is also triggered by stress transfer processes during dyke intrusive events (Walter et al., 2005; Bonforte et al., 2019, Alparone et al., 2020, Mattia et al., 2020).

Fault rupture related to aseismic creep on Mt. Etna has been known since the end of the 19th century (Silvestri, 1879), with episodic events localized in some fault segments of the SE flank (Fig. 1a) that cause damage to buildings and roads. Aseismic creep certainly plays a role in the volcano-tectonics of Etna volcano, and to better understand it, in this paper we analyse two events at Santa Tecla using a multidisciplinary approach. Santa Tecla is a small coastal village crossed by 3 active faults: the Santa Tecla, Guzzi and Scalo Pennisi (ITHACA Working Group, 2019; see location in Fig, 1a). In particular, we present the first in-depth study along the Scalo Pennisi Fault (SCA in Fig. 1a), providing an accurate map of the surface faulting related to episodic aseismic creep events. Furthermore, we mapped the 2002 coseismic ground ruptures along the Santa Venerina (VEN), San Giovanni Bosco (BOS), Guzzi (GUZ), Scillichenti (SCI) and Guardia (GUA) Faults (see location in Fig. 1a). We mapped the 2022 and the 2002 ground rupture events and collected structural data, displacement, length and pattern of ground breaks. We used published seismological, geodetic and InSAR data for interpretation of the 2002 surface faulting events. We performed an InSAR analysis for the 2022 creep event, decomposing the LOS displacement in the horizontal and vertical component of deformation. We used the data collected in the field to constrain the fault model obtained by the InSAR inversion using the GBIS software (Bagnardi and Hooper, 2018).

We processed the collected data to evaluate the SCA Fault geometry and surface faulting hazard. Then we discuss the concurrent role of the aseismic creep in the lower eastern flank of Mt. Etna, and in context of volcano-tectonic and gravitational processes.

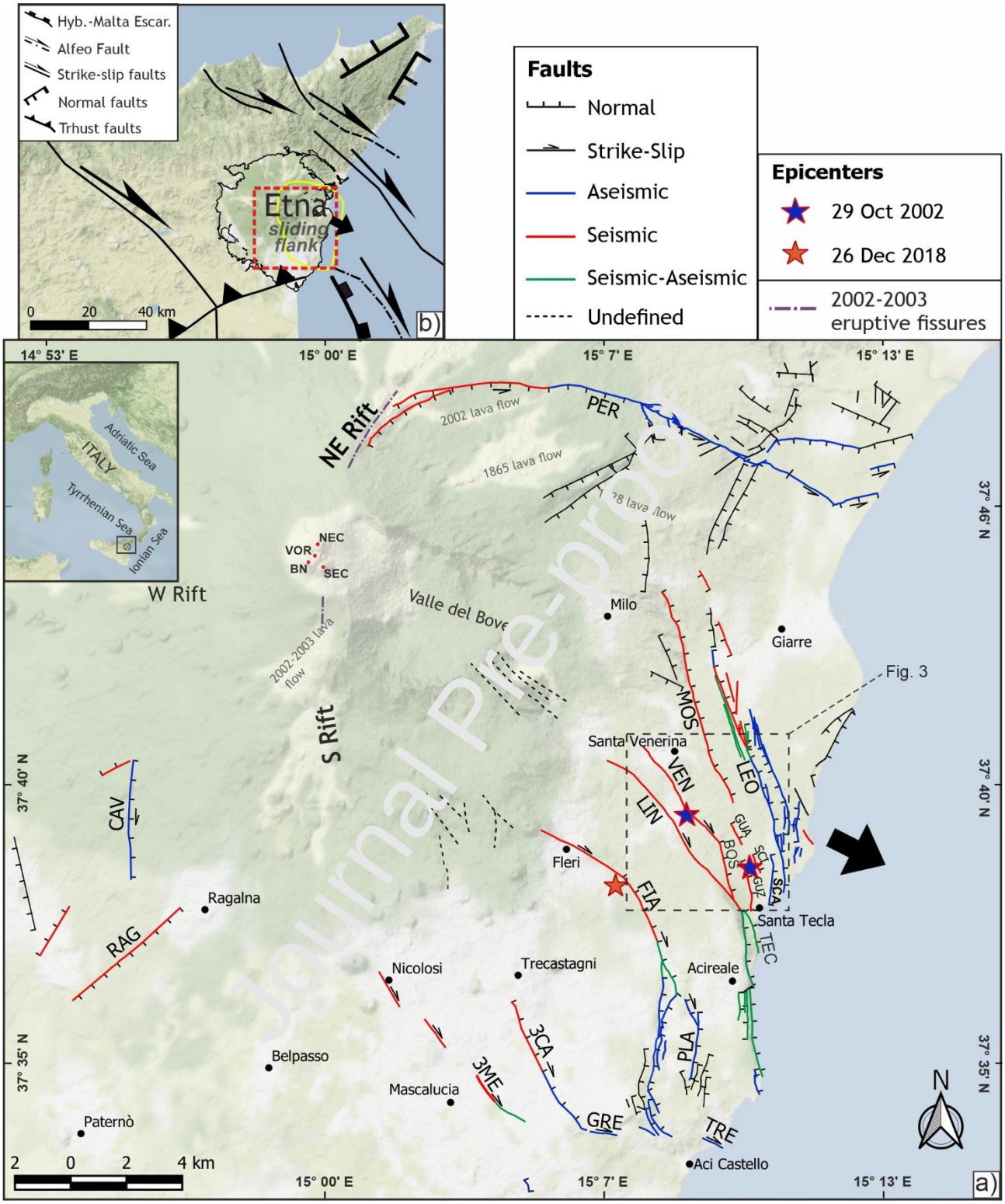

Figure 1: a) General map of Mt. Etna showing active and capable faults kinematics (ITHACA Working Group, 2019) and seismic/aseismic behaviour (modified from Azzaro et al., 2012); orange and blue asterisks are the epicenters of last surface faulting earthquakes (2018 Fleri, 2002 Santa Venerina and Scillichenti; from CPTI15, 2022); the white coloured sectors are the urbanized areas. The dashed rectangle shows the location of Figure 3. Fault codes: SCA: Scalo Pennisi; GUZ: Guzzi; SCI: Scillichenti; VEN: Santa Venerina; BOS: San Gjovanni Bosco; FIA: Fiandaca; LIN: Linera; TEC: Santa Tecla; MOS: Moscarello; GUA: Guardia; LEO: San Leonardello; PLA: Aci Platani; TRE: Aci Trezza; GRE: San Gregorio; 3CA: Trecastagni; 3ME: Tremestieri; RAG: Ragalna; CAV: Masseria Cavaliere; PER: Pernicana. Etna summit craters are labelled as follow: VOR: Voragine; BN: Bocca Nuova; NEC: NE crater; SEC: SE crater. b) tectonic framework of NE Sicily (simplified from Gross et al., 2016 and Polonia et al., 2016) with Etna volcanic edifice outlined by the black line (Branca et al., 2011) and its eastern sliding flank.

2. Geologic and seismotectonic setting

Mt. Etna volcano is located on the Appennine-Maghrebian thrust and fold belt, in a complex geological framework (Fig 1b). Mt. Etna is characterized by effusive and explosive activity with basaltic lava flows from the summit craters and also from fissures and scoria cones formed along its flanks. The flank eruptions are mostly located along the so-called S and NE rifts (Fig. 1a). According to Branca et al. (2011), the current volcanic edifice started building over the last 110 ka, creating the Valle del Bove volcanoes (110-65 ka), followed by the Ellittico (65-15 ka) and Mongibello volcanoes (15 ka-present). The volcanic succession along the SE flank lies above the Early-Middle Pleistocene blue marly clay (i.e.., Argille grigio-azzurre formation; Branca et al., 2011) of the sedimentary basement. Along the eastern slope the thickness of the volcanic succession reaches maximum values of about 600 m where there are depressions in the sedimentary basement, but thickness generally decreases approaching the coastline (Branca and Ferrara, 2013). The study area of these investigations is in the SE flank (Fig. 1a), where the prehistoric Mongibello lava flows covered the Timpe (180-11l.0 ka; Branca et al., 2011) and Ellittico volcanic products formed a complex coastline in the area where Santa Tecla is presently located. The volcanic succession in the San Giovanni Bosco area and to the S of Santa Tecla reaches thicknesses of ~600 m because it lies above the deepest depression of the sedimentary basement (Branca and Ferrara, 2013).

The eastern and southern flanks of the volcano are affected by active normal, strike-slip and oblique-slip faults (Fig. 1a) as interpreted from surface faulting features and focal mechanisms (Azzaro, 1999; Scarfì et al., 2013). In particular, there are 4 main fault systems. 1) the left lateral Pernicana Fault (PER) to the NE; 2) the right lateral Tremestieri (3ME) – Trecastagni (3CA) – San Gregorio (GRE) – Aci Trezza (TRE) Faults to the S; 3) the Timpe Fault system to the E with normal and right lateral motion; 4) the Ragalna (RAG) and Masseria Cavaliere (CAV) Faults to the SW (see Fig. 1a for the faults location). The Timpe Fault system includes the following faults: San Leonardello (LEO), Moscarello (MOS), Guardia (GUA), Scillichenti (SCI), Guzzi (GUZ), Scalo Pennisi (SCA), Santa Venerina (VEN), San Giovanni Bosco (BOS), Linera (LIN), Santa Tecla (TEC), Fiandaca (FIA), Aci Platani (PLA; see locations in Fig. 1). These capable faults are characterized by moderate magnitude seismicity (Mw<5), shallow earthquake foci (<1 km), and they typically have segments with both coseismic and aseismic creep ruptures (Fig. 1a; Rasà et al., 1996; Azzaro et al., 2012; Mattia et al., 2015). Gravity plays a concurrent role in driving the shallow deformation (Rasà et al, 1996, Tibaldi and Groppelli, 2002) that is also influenced by the morphology of the sedimentary basement and the thickness of the volcanic pile (Tringali et al., 2023).

The highest magnitude historical earthquakes with significant surface faulting occurred along the Timpe Fault System (e. g., Fiandaca, Linera, Santa Venerina and Moscarello; Fig. 1a) where the thickness of the volcanic pile is the greatest considering the Etna eastern flank (Branca and Ferrara, 2013), reaching intensity IX (Azzaro, 1999) on the European Macroseismic Scale (EMS-98; Grünthal, 1998). These earthquakes are typically very shallow with hypocentral depth typically less than 1 km. Most building damage occurs within a 1-2 km wide band around the causative fault and it is essentially linked to the surface faulting. The last two strong seismic events (see location in Fig. 1a) occurred in 2002 along the Santa Venerina Fault (Mw 4.4) and

in 2018 along the Fiandaca Fault (Mw 4.9), both during dike intrusions and flank eruptions.

Aseismic creep events often occur after earthquakes, typically in the framework of dyke intrusions, but also in different patterns. Azzaro et al. (2020) observed that in May 2009, an aseismic creep in the S sector of the San Leonardello Fault preceded a Mw 4.0 earthquake along the N sector. This kind of behaviour suggests that the aseismic creep in a fault segment can load the rest of the tectonic structure (Azzaro et al., 2020). In particular, creep events commonly occur along the coast (Fig. 1a), where the blue marly clay basement is higher and the thickness of the volcanic pile decreases.

Along the Mt. Etna SE flank, the fault systems accommodate the slow gravitational sliding toward the sea (Bonforte et al., 2011). The collapsing sector is between the Pernicana Fault to the NE and the Tremestieri – Trecastagni – San Gregorio – Aci Trezza Faults to the S. These faults are specifically located where the basement forms two ridges, the Vena Ridge to the NE and the Aci Trezza Ridge to the S (Branca and Ferrara, 2013). In recent years, multibeam and seismic reflection investigations indicate that deformation is also active in the offshore sector (Chiocci et al., 2011; Gross et al., 2016; Urlaub et al., 2022). Aci Trezza Fault and some Timpe Faults have a clear prolongation in the Ionian Sea (Gross et al., 2016). An episodic aseismic creep event was recorded in 2016 along the offshore prolongation of the Aci Trezza Fault with 4 cm of aseismic slip (Urlaub et al., 2018).

The creep events documented in this study occurred along the SCA Fault characterized by: 1) a total length of about 1,8 km; 2) an arcuate trace changing its strike from N190° to the S, to N350° to the N; 3) E dipping normal kinematic. We documented also the coseismic surface faulting of the 29 October 2002 earthquakes occurred along the Santa Venerina and Guzzi Faults. A strong earthquake of intensity VIII-IX on the EMS-98 scale occurred along the Santa Venerina Fault on 17 June 1879 with associated 4-6 km of surface faulting (Silvestri, 1879a; Azzaro, 1999 and references therein). Santa Venerina Fault is characterized by: 1) a total length of about 4.5 km; 2) Strike N320°; 3) transtensive dextral kinematic. Santa Venerina Fault is connected in its SE portion to the San Giovanni Bosco Fault characterized by: 1) a total length of 2 km; 2) strike N350°; 3) normal kinematic with right lateral component. Small earthquakes with surface faulting occurred along the San Giovanni Bosco Fault in 1909 (Riccò, 1909) and 1986 (Azzaro, 1999 and references therein). Guzzi Fault along with the Guardia and Scillichenti Faults are considered S stepping en-echelon splays of the Moscarello Fault (Azzaro et al., 2012).

3. Materials and methods

4.1. Field survey and dataset compilation

We surveyed the ground ruptures along the activated fault segments in 2002 and 2022, collecting data mostly along roads, walls and pavements. Our survey started after the 29 October 2002 main shock in the Santa Venerina area, moving to the Santa Tecla village during the afternoon after the Scillichenti earthquake. We mapped the creep in Santa Tecla the day after the seismic event, and residents informed us that the ruptures began to open about an hour after the Scillichenti earthquake. We conducted periodic survey, every 3 months, along the faults in the area to monitor the

displacement variations along the ground ruptures. The day after the aseismic creep event, on 9 February 2022, we commenced a 10 day survey. Over the following six months, we checked each week to establish whether there was variation in the measured displacements at each location. The ground breaks were mapped using topographic maps at 1:2000 scale or by means of digital mapping devices with built-in navigation-grade GNSS systems and using high-resolution satellite images as basemaps. Using a geological compass and tape ruler, we measured the following data along the ruptures: strike, length (m), heave (i.e., horizontal displacement in cm), throw (i.e., vertical displacement in cm), net slip displacement (cm), slip trend and plunge from certain piercing points. The dataset is available in the zenodo repository (https://doi.org/10.5281/zenodo.7263296).

4.2. Radar interferometry and Geodetic Bayesian inversion

We detected ground motions during the creeping event of 2022 by means of radar interferometry. We selected Sentinel-1 pairs in both ascending and descending orbits (Descending 29 Jan-10 Feb 2022; Ascending 4-20 Feb 2022) encompassing the desired time window (further details in supplementary material).

SAR Interferometric images (InSAR) were calculated with the SNAP software suite, by means of a standard TOPSAR interferometric workflow. A 10x2 multilooking and a Goldstein filter have been applied to increase the signal to noise ratio and to increase data correlation, resulting in a ca. 40 m spaced grid in ground resolution. Line of Sight (LOS) movements have been decomposed in the vertical and E-W components, according to the following formulas (Mancini et al., 2021):

$$\begin{bmatrix} D_{up} \\ D_{EW} \end{bmatrix} = A^{-1} \begin{bmatrix} D_{LOS}^{asc} \\ D_{LOS}^{desc} \end{bmatrix}$$

with

$$A = \begin{bmatrix} \cos(\theta_{asc}) & \sin(\theta_{asc})\cos(\alpha_{asc}) \\ \cos(\theta_{desc}) & -\sin(\theta_{desc})\cos(\alpha_{desc}) \end{bmatrix}$$

where D_{up} and D_{EW} are the vertical and E-W horizontal displacements, θ indicate the incidence angles and α the heading angle for both ascending (*asc*) and descending (*desc*) observations.

We used the Geodetic Bayesian Inversion Software – GBIS v.1.1 (Bagnardi and Hooper, 2018; https://comet.nerc.ac.uk/gbis/) to perform non-linear homogeneous-slip inversion of the best-fit fault geometry and parameters that induced the observed creeping event.

Following the same procedure of Bagnardi et al. (2018), we sub-sampled the original dataset with a Quadtree resampling method (original datasets and subsampled deformations fields are available in Supplementary Fig. 2) to reduce the number of measurement points to be inverted (i.e., n. 62 and 58 points for the ascending and descending pairs, respectively).

After subsampling the InSAR data, the theoretical covariance function was estimated using the experimental semivariogram, which was used to populate the variance-covariance matrix, according to the distance between the polygon centroids (Fig. 2). The two analyzed pairs show very limited values of ground movement, close to the lower limit of detection of the InSAR techniques in C band. Nonetheless, variance/covariance analysis of the measured deformation shows that, especially for the ascending pair, data are spatially correlated inside the area of deformation, whereas an almost linear trend dominates outside of it (Figs. 2a and b). Covariance

matrix maps (Fig. 2c) show positive values with a stronger covariance associated with the ascending InSAR.

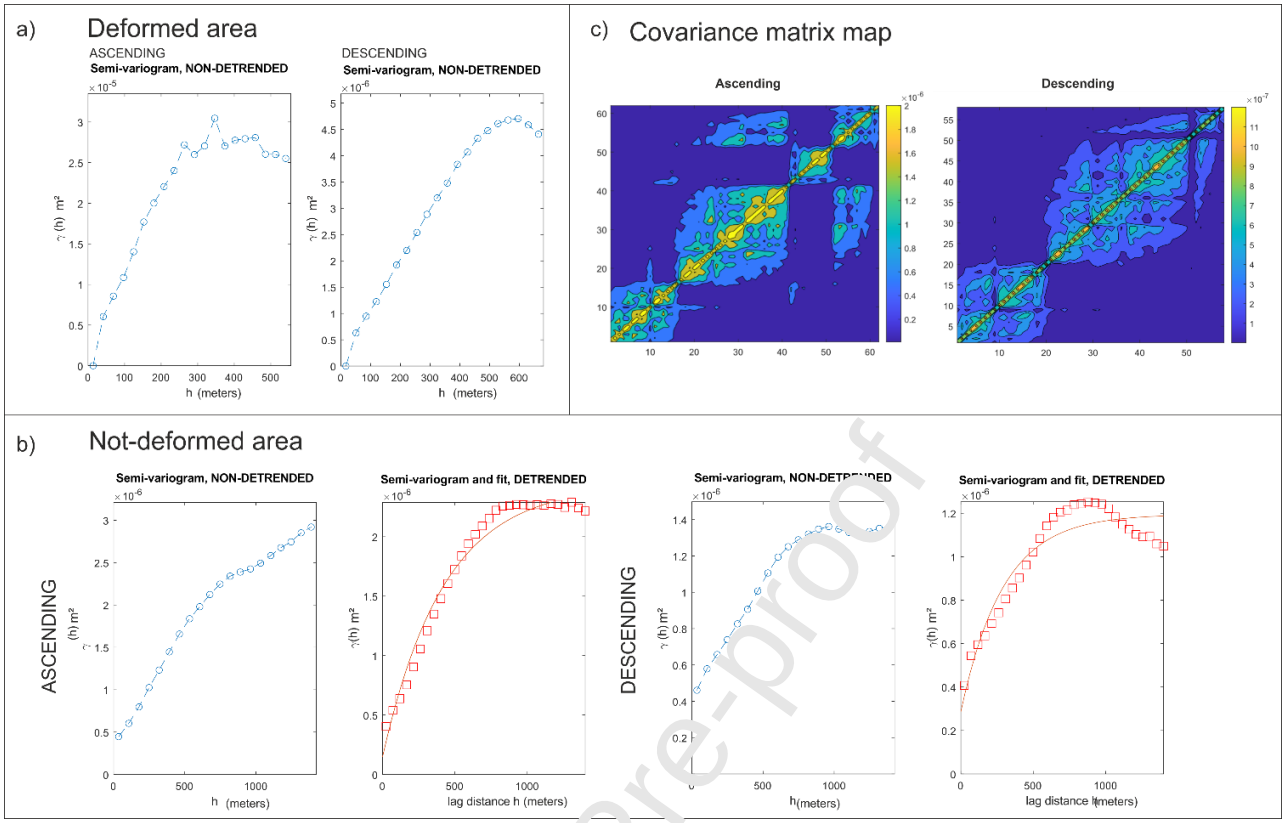

Figure 2: Variance analysis of the InSAR pairs (ascending and descending) used for inversion: a) variogram of the deformed area; b) variogram of the not-deformed area before and after linear detrending; c) covariance matrix maps for the ascending (n. 62 measured pixels) and descending (n. 58 measured pixels) pairs.

Inversions and forward deformations of the fault are calculated in an elastic half-space (Okada, 1985), where preliminary Poisson ratio and shear modulus are set to 0.25 and 3.32×10^{10} N/m^2, respectively. The fault model is rectangular in shape with a uniform slip distributed on the plane; the operator sets the possible range of the inverted variables, the step size and the maximum number of run models. The search parameters for the fault are: location (i.e., X, Y and Z and the midpoint of the upper tip of the fault plane), dimensions (i.e., length and width), orientation (i.e., strike and dip) and dip-slip and strike-slip components of the slip on the fault. GBIS runs the indicated number of runs (here set at $1 \cdot 10^6$ models) and then uses a Bayesian probabilistic inversion algorithm where an optimal set of fault parameters are calculated from the a-posteriori probability density functions (PDF). See Bagnardi and Hooper (2018) for further details.

4. The 29 October 2002 surface faulting events

During the period October 2002-January 2003, a seismic swarm accompanied a dyke intrusion and an eruptive event (i.e., 2002-2003 Etna eruption) developed with the opening of eruptive fissures in the Etna NE and S Rifts. On 26 October 2002, the seismic swarm begun in the summit craters area of the Etna volcano with the earthquake foci elongated along N-S direction until 27 October, when the seismicity migrated in the NE Rift and along the Pernicana Fault (Barberi et al., 2004). On 29 October, the seismicity moved also in the eastern flank of the volcano along the Timpe Fault system, with most of the earthquakes foci at less than 2 km depth

(Barberi et al., 2004). The Mw 4.4 main shock occurred at 11:02 (local time) along the Santa Venerina (VEN) Fault, producing 5 km of surface faulting (Fig. 3 and Supplementary Figs 3, 4 and 5; Monaco et al., 2005; Blumetti et al., 2007; Azzaro et al., 2012), including the northern part of the San Giovanni Bosco (BOS) Fault. At 17:39 (local time) a Mw 4.0 seismic event (i. e., Scillichenti earthquake) occurred in the lower eastern flank of the volcano, producing about 3 km of discontinuous surface faulting along the Guzzi (GUZ), Scillichenti (SCI) and Guardia (GUA) Faults (Fig 3; Monaco et al., 2005; Blumetti et al., 2007). About an hour after the Scillichenti earthquake, an episodic aseismic creep event occurred along the SCA Fault.

The western area of Santa Venerina showed small tensional Riedel fractures with heave up to 1 cm, mainly arranged with a left-stepping en-echelon pattern, indicating a dextral transtensive kinematic (Figs. 3 and 4). The maximum slip values (heave up to 50 cm, throw up to 20 cm and 2-10 cm of right lateral offset) were observed in the SE part of the Santa Venerina Fault and in the N sector of the San Giovanni Bosco Fault with slip vector trend between 90° and 120° (Fig. 3a). The ground ruptures of the Scillichenti earthquake showed a throw up to 5 cm and heave up to 50 cm (Figs. 3 and 4d) with slip vector trend between 85° and 100°. The coseismic ground ruptures damaged the water supply network in many locations (Blumetti et al., 2007). At Santa Tecla, the aseismic creep event produced 350 m of surface faulting in the S sector of the SCA fault (Fig. 3 and 5), with the formation of two parallel ground breaks delimiting a 2-5 m wide graben along the roads crossed by the fault. The average strike of the ruptures was N190° (Fig. 5) with slip trend toward the E. The ruptures showed heave and throw of up to 1 cm. We observed that the creep event continued in the S part of the fault at least until November 2005, reaching the maximum heave and throw of 2 cm. Between the end of 2002 and 2004, we also observed a weak reactivation of the Santa Tecla Fault (TEC in Fig. 1a and 3a) with maximum slip values of 0,8 cm reached.

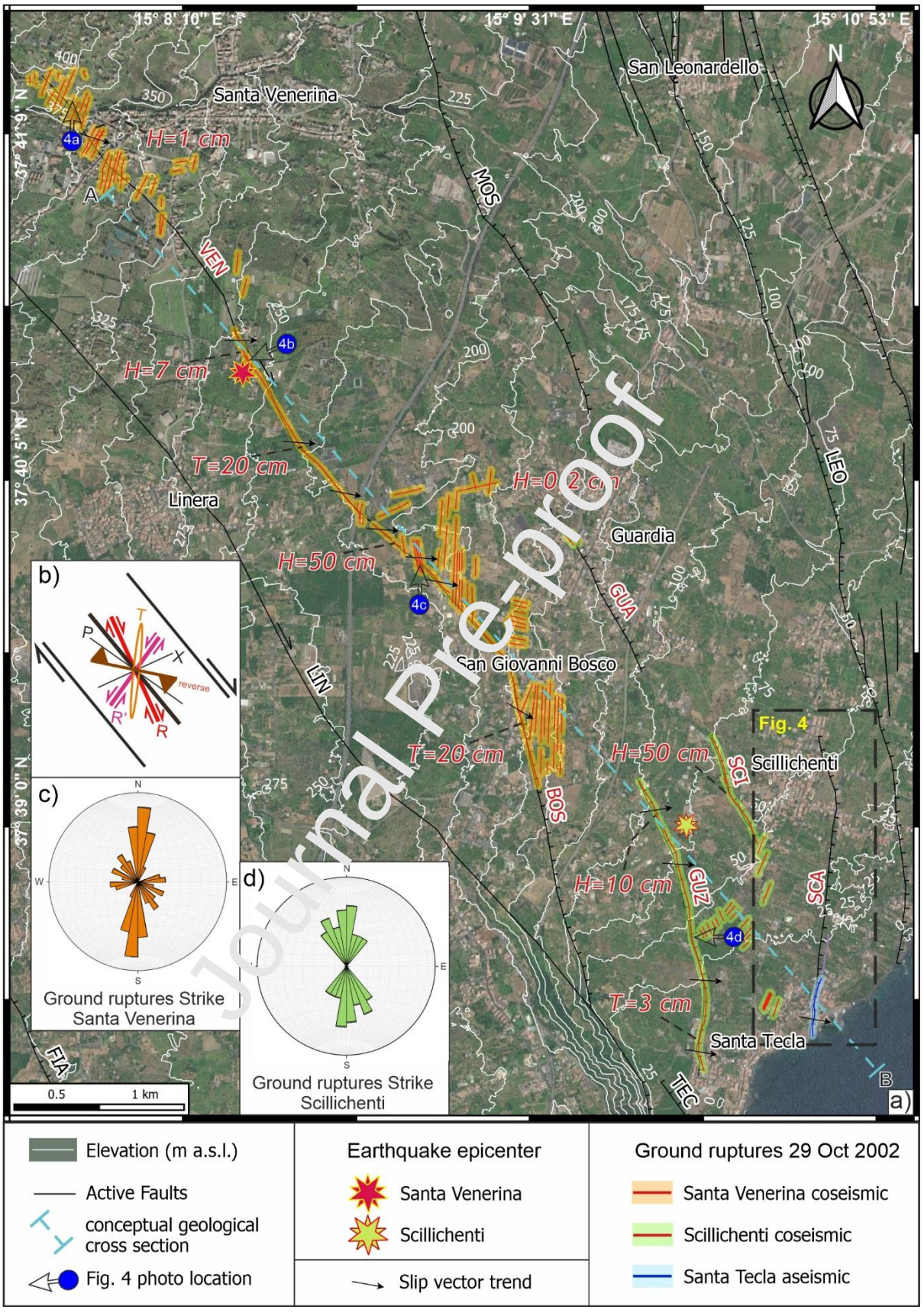

Figure 3: a) 29 October 2002 ground ruptures map with relative maximum displacement values (H=Heave; T=Throw); b) Riedel model of right simple shear; c and d are the related rose diagram with strike distribution for each earthquake.

Figure 4: Field photos (taken between 29-31 October 2002) of the surface ruptures related to the Santa Venerina and Scillichenti earthquakes, locations in figure 3. a) ground break along a road and a concrete wall in the W side of Santa Venerina; b) ground rupture on a secondary road and collapse of a dry wall; c) ground cracks affecting a road and a wall in the NW side of San Giovanni Bosco; d) large crack on the soil to the S of Scillichenti.

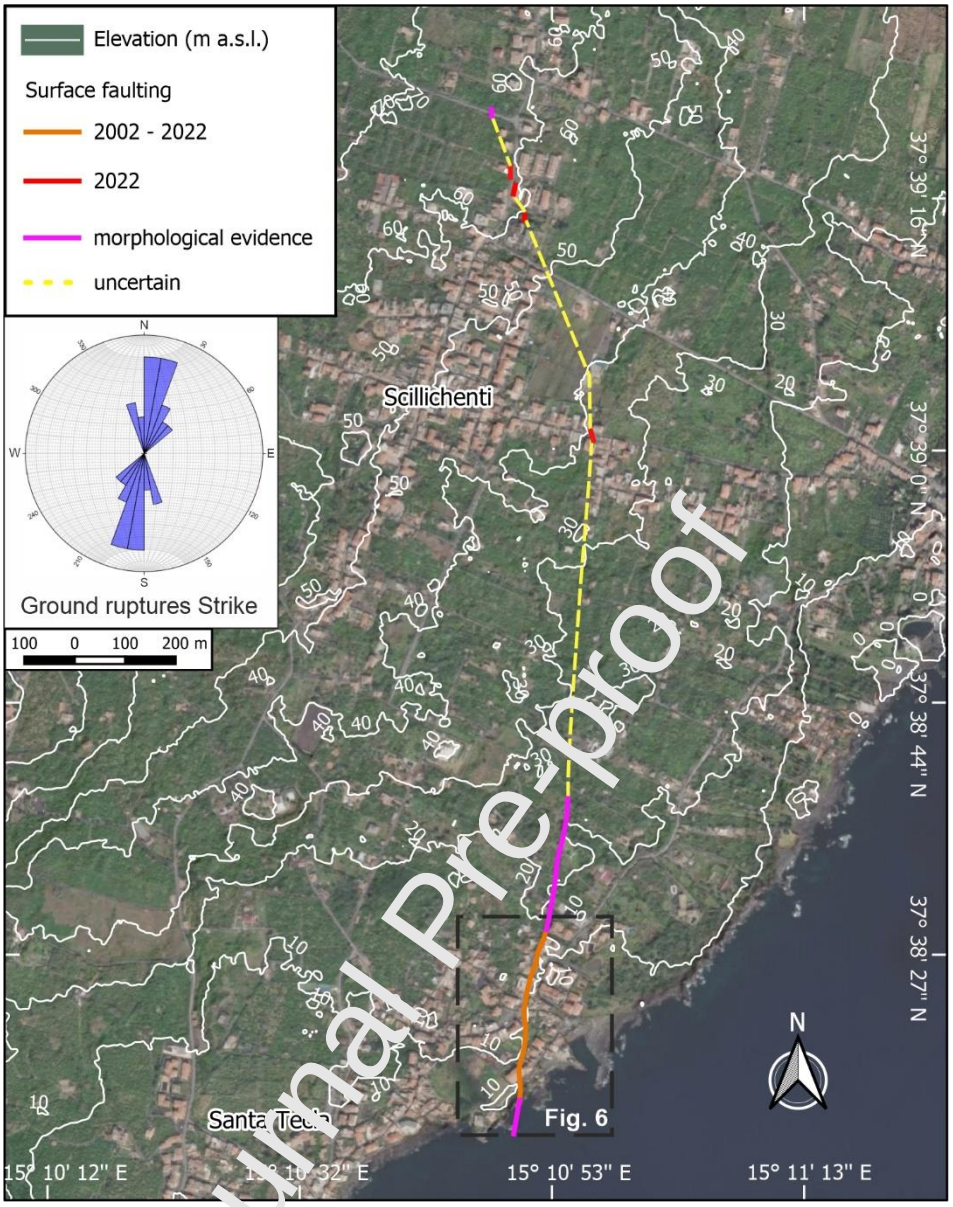

Figure 5: Map showing the surface faulting between Santa Tecla and Scillichenti, produced along the SCA Fault during the 2002 and 2022 aseismic creep events.

5. The 8 February 2022 SCA Fault aseismic creep event

5.1 Surface faulting

On 8 February 2022, the lower eastern flank of the Mt. Etna volcano experienced episodic aseismic creep along the Scalo Pennisi Fault. The creep had various effects, including the reopening of pre-existing ground ruptures, and minor damage to buildings and roads as well as waterpipe breakage in the northern part of the Santa Tecla hamlet (Fig. 6). According to the local residents' statements, the creep also produced 3 tremors at one-hour intervals starting at 9:00 p.m (local time), on 8 February.

In the morning of 9 February, we started to map the ruptures produced by the creep, and we observed the reopening of the 2002 ground breaks, and we assessed some minor new ruptures along roads and buildings (Figs. 6 and 7). We could follow a nearly continuous ground rupture trace for about 350 m. In the farmland N

of Santa Tecla, we surveyed damage in walls and documented fault morphological features such as graben about 2 m wide but without new clear ground ruptures (Fig. 5). The average strike measured was N190° with heave and throw generally less than 1 cm (Table 1; Figs. 6 and 7). We noticed that the building damage had increased since 2002 as shown in Fig. 7e. We observed the formation of new ground cracks in roads and walls with heave <0,5 cm in the northern part of the fault located to the E and N of the Scillichenti village (Fig. 5).

Local residents reported that an episodic aseismic creep had occurred in the same area with damage to buildings at the end of the 1970s. The creep event interested the S sector of the SCA Fault lactide in the NE part of Santa Tecla. A summary of the episodic aseismic creep events along the SCA Fault is shown in Table 1.

Date	Locality	Strike	Kinematic	Length (m)	Max Heave (cm)	Max Throw (cm)	Ref.
Late 1970s	Santa Tecla	-	Normal	-	-	-	Local witnesses
29 Oct 2002-Nov 2005	Santa Tecla	N190°	Normal	350	1-2	1-2	This study
8 Feb 2022	Santa Tecla	N190°	Normal	350	1	0-1	This study

Table 1: Known episodic aseismic creep events along the SCA Fault.

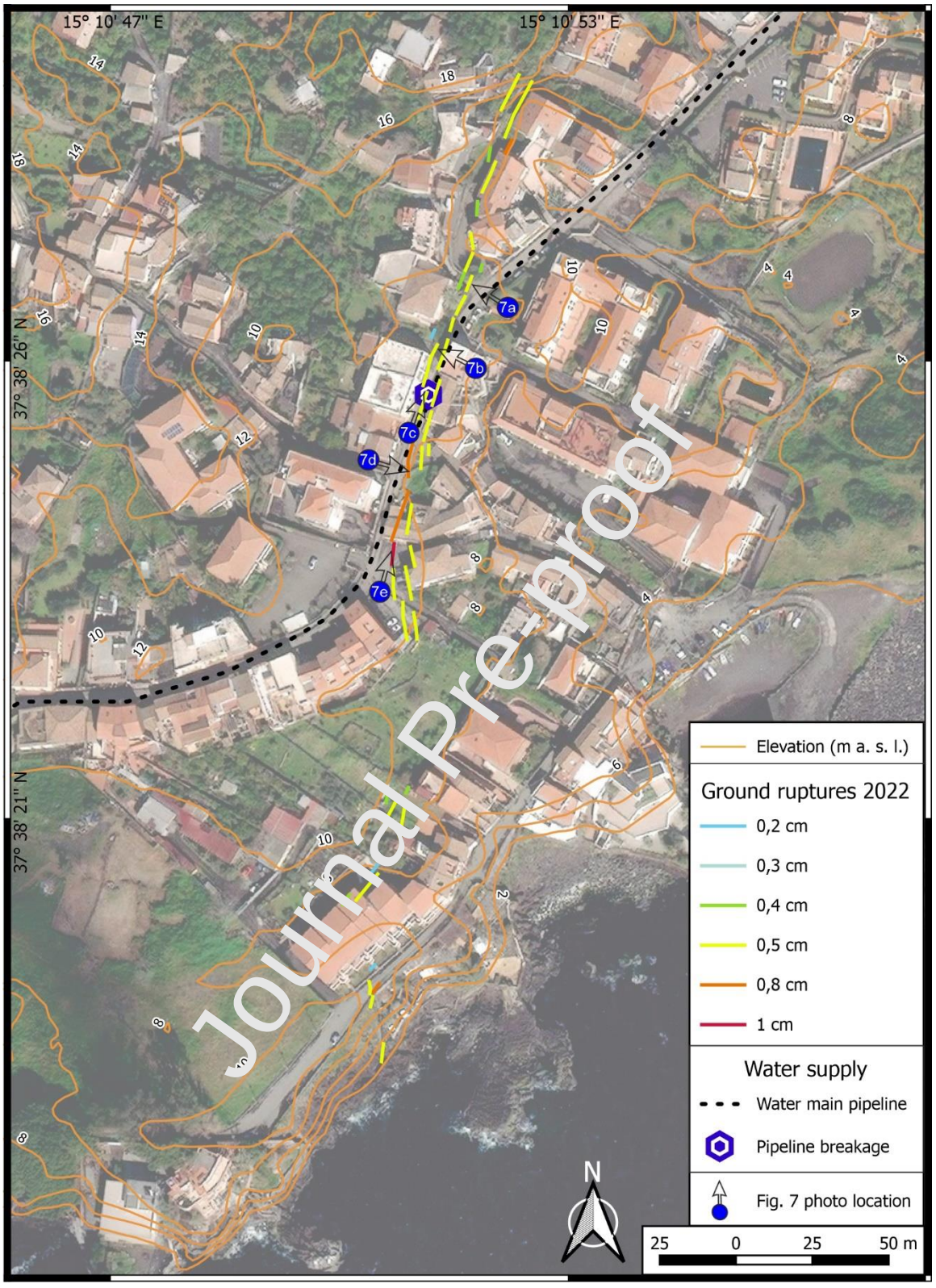

Figure 6: Ground ruptures mapped in Santa Tecla after the 8 February 2022, color-coded according to the heave amount; the black dashed line is the water main pipeline which was broken where it crosses the SCA Fault; blue dots are the photo locations showed in Fig. 7, the arrow indicates the direction of the photo shoot.

Figure 7: Field photos of the ground breaks (see blue points in Fig. 6 for location): a) fractures on pavements and walls of a secondary road; b) gate displaced by the fault creep; c) main and antithetic faults delimiting a graben; d) fracture on a wall with displaced musk; e) building damaged and accumulated displacement between the road basaltic tiles.

5.2 InSAR-detected ground deformation and GBIS inversion

Both the InSAR ascending and descending observations (Fig. 8a and b) indicate an area of narrow deformation, with an overall LOS movement of less than one sensor wavelength (i.e., ca, 5.54 cm) that is centered on the SCA Fault. Only a fraction of the total deformed area is included in the onshore sector, being apparently close to half of it, given the symmetry in the map view footprint of the deformed sector (Fig. 8a and b). Nonetheless, we cannot exclude a slightly greater deformed area, basing on the available observations.

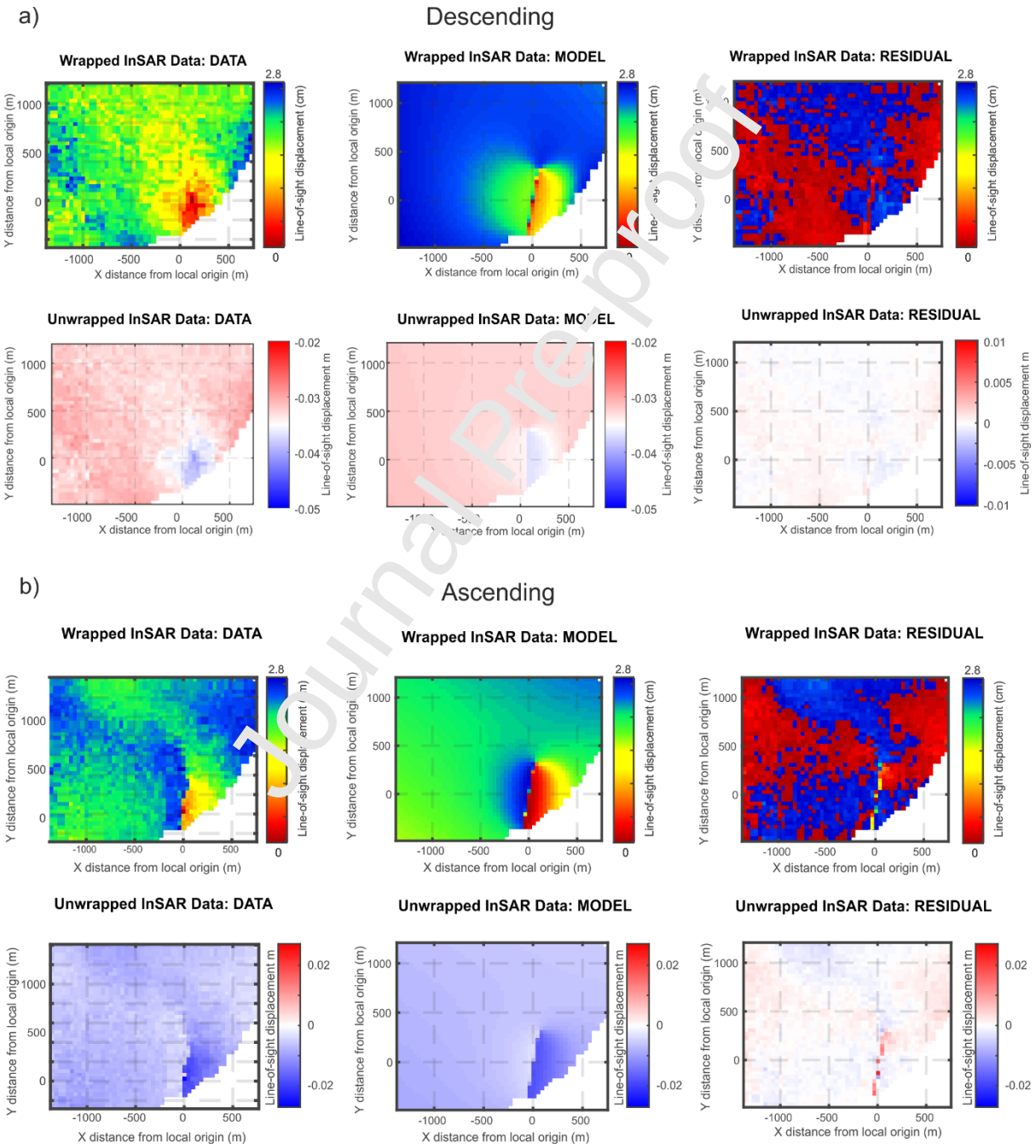

Figure 8: Results from the inversion of the InSAR Sentinel-1 pairs; a) descending and b) ascending pairs.

We calculated vertical and E-W components along a profile transect across the deformed area and oriented close to the location of the maximum measured offset (Fig.9). The decomposition reveals a subsiding and eastward-moving sector, to the E of the SCA Fault (Fig. 9c, d and e), consistently associated with the deformation field expected from an E-dipping normal fault. The width of the deformed area suggests a relatively shallow displacement source, corroborated by the inversion analysis.

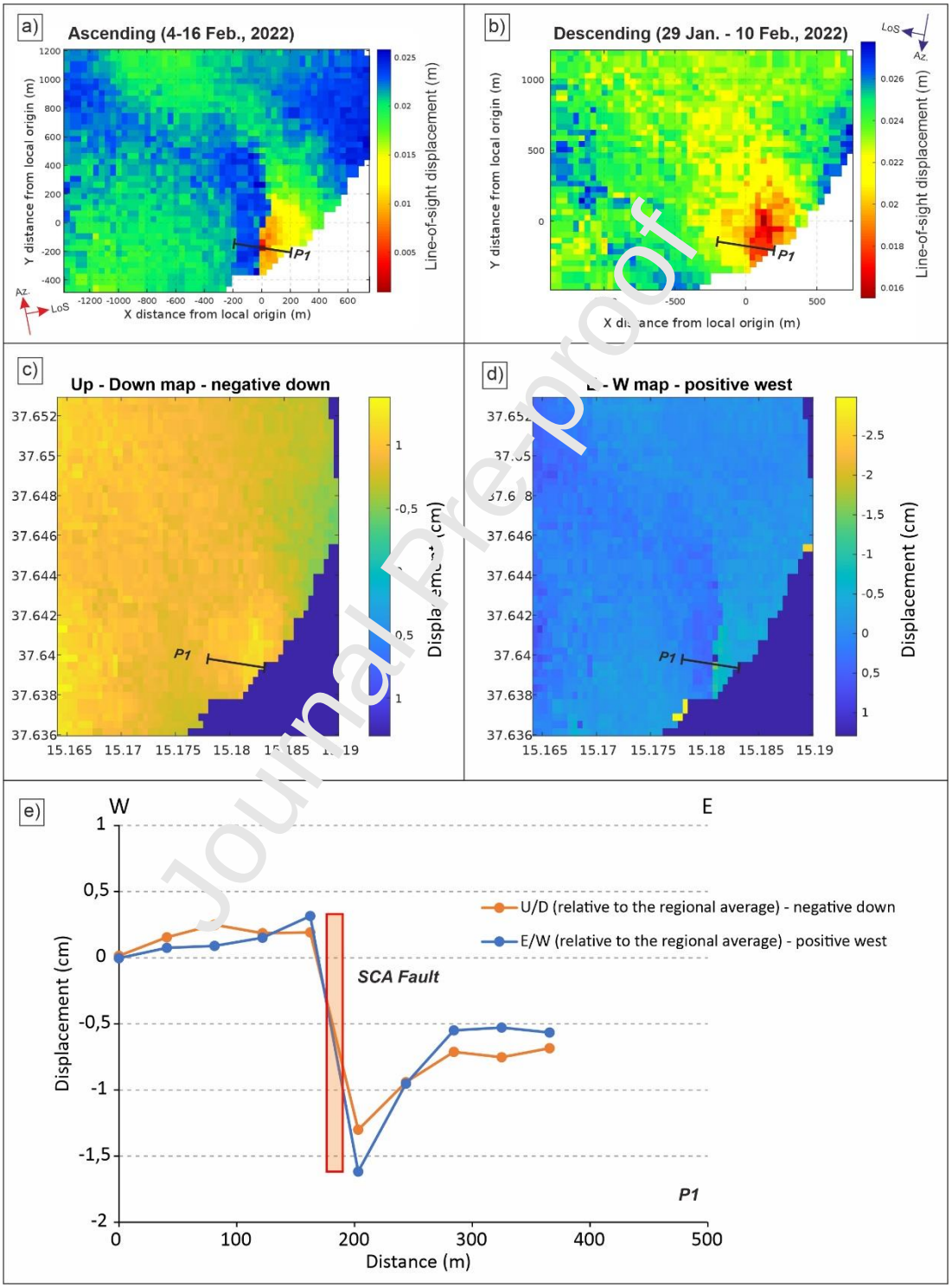

Figure 9: wrapped LOS displacement for ascending (a) and descending (b) observations. c) Up-Down component map; d) E-W component map e) LOS velocities decomposition along the profile P1.

Using the GBIS software platform, we ran models with different combinations of fault parameters within the range of values listed in Table 2. We set a wide range of values, except for strike, which is constrained by our field mapping observations (i.e., N190).

Bayesian inversion (see Supplementary Material) resulted in best fit optimal values and confidence intervals (Table 2) that were consistent with an east-dipping normal fault. The best fit fault is ca. 700 m long and 500 m wide, dipping ca. 43° to the E. The upper fault tip is very close to the ground surface (ca. 3 meters depth) and the rupture extends down to an estimated depth of ca. 300 m. Optimal values are well constrained by the inversion, especially considering the depth of the fault's upper tip and the fault dip. Possibly, the source could have a greater value in fault length if the source center is moved accordingly more to the south (see the Convergence Plots and the Joint Probabilities Plot in the Supplementary Material). In any case, the calculated solutions delimit the fault length within a maximum value close to ca. 1200 m (Table 2).

Parameter	*Min – Max*	*Step*	*Optimal*	*Mean*	*Median*	*2.5%*	*97.5%*
Fault Length (m)	300 - 5000	100	**714.83**	791.14	736.31	589.46	1266.38
Fault Width (m)	100 - 5000	100	**518.97**	603.51	560.02	439.72	856.60
Depth of the fault upper tip (m)	0 - 10000	100	**2.56**	88.56	2.95	0.18	11.04
Dip (°)	0 - 90	1	**-42.74**	-44.13	-44.00	-51.11	-37.86
Strike (°)	Fixed 190	1	**-**	-	-	-	-
Upper tip Midpoint - X (m)	-500 - 500	50	**-19.86**	-20.01	-19.84	-58.90	6.20
Upper tip Midpoint - Y (m)	-500 - 500	50	**-55.27**	-91.17	-74.08	-351.58	0.51
Strike slip component (m) (positive if dextral)	0 – 0.2	0.01	**0.00**	0.00	0.00	0.00	0.01
Dip slip component (m) (positive if normal)	-0.2 – 0.2	0.01	**0.02**	0.02	0.02	0.01	0.02

Table 2: search range of the inverted parameters and results; for further details, refer to the Supplementary Material.

6. Discussions

In order to understand the depth of detachment of the SCA Fault obtained with GBIS, we analysed: 1) the seismic and volcanic activity of Mt. Etna during the 2002 and 2022 aseismic creep events; 2) surface geology (Branca et al., 2011) and thickness of the volcanic pile; 3) depth of the sedimentary basement (Branca and Ferrara, 2013).

The 2002 SCA aseismic creep event was accompanied by a seismic swarm and dyke intrusion with earthquakes and surface faulting mainly along the Pernicana, Santa Venerina and Guzzi Faults. In particular, the two strongest seismic events along the Timpe Fault system were very shallow (Fig. 9): 1) the Santa Venerina earthquake foci was at 50 m b.s.l. (Alparone et al., 2015), with the basement at 275 m b.s.l. (Branca and Ferrara, 2013); 2) the Scillichenti seismic event had an hypocentral depth of 220 m b.s.l. (Alparone et al., 2015), with the basement at 500 m b.s.l. (Branca and Ferrara 2013). In both cases the rupture occurred within the volcanic pile (Fig. 10) as in the 26 December 2018 Fleri earthquake (Tringali et al., 2023). These hypocentral depths suggest that the seismogenic layer, capable of causing moderate-magnitude (Mw>4) earthquakes with surface faulting, is limited within the volcanic pile (Tringali et al. 2023).

Furthermore, the maximum displacements related to the Santa Venerina earthquake, in particular the throw, were observed in the San Giovanni Bosco area (Fig. 3), where the maximum thickness of the volcanic pile is reached as observed also for the Fleri earthquake (Tringali et al., 2023). The different rheology of the volcanic rocks and the blue marly clay layers probably led to decoupled deformation processes. If we consider the vertical uncertainty of the hypocentral depths, 600 m for Santa Venerina and 300 m for Scillichenti (Fig. 10), the rupture could have been at the interface between the volcanic rocks and the basement, suggesting a SE sliding of the volcanic pile on the blue marly clays, as was proposed for the 2018 Fleri earthquake (Tringali et al., 2023). Certainly, the rupture could be within the clay basement, but it would still less than 1 km in depth, lying above the hypothetical detachment surface proposed in the literature (2-3 km; Puglisi et al., 2008; Siniscalchi et al., 2012). The latter scenario could suggest the presence of at least two detachment surfaces at different depths, shallow and deep, that could act also at the same time, as already suggested in previous studies (Acocella et al., 2003; Rust et al., 2005). Moreover, the 2002-2003 seismic swarm was preceded and followed by an acceleration of the E flank sliding, until 2005, which had never been observed before, with a shift to the SE as demonstrated by InSAR and GNSS deformation data (Acocella et al., 2003; Bonaccorso et al., 2006; Neri et al., 2009). Geodetic data are consistent with our observations in the field, with fault rupture propagation to the SE and slow continuation of aseismic creep along the Santa Tecla (TEC in Fig. 1a) and SCA Faults during the period November 2002-November 2005. In summary, these data suggest sliding of the E flank toward the SE, as proposed by Neri et al. (2004) regarding the extensive surface faulting observed along the Pernicana Fault during the period 2002-2003. A similar behaviour was observed following the seismic swarm and eruption in December 2018 with an abrupt acceleration of flank instability (Alparone et al., 2020; Mattia et. al., 2020) and considering that aseismic creep along the Aci Platani Fault (PLA in Fig. 1a) continued slowly for about a month (Tringali et al., 2023), accumulating an additional cm of slip.

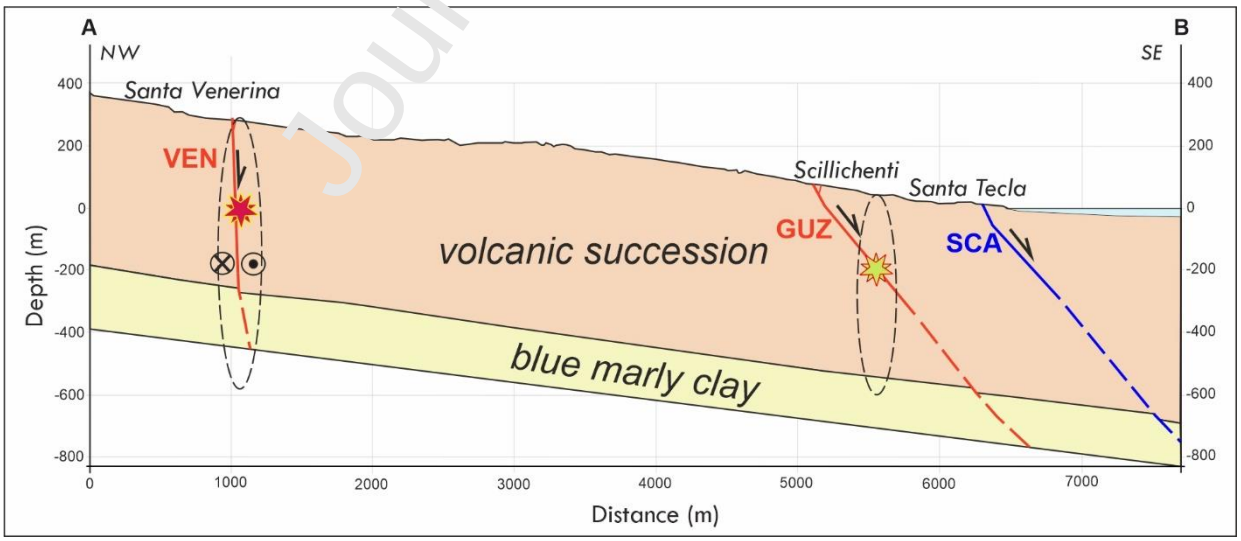

Figure 10: Conceptual geological cross section (location in Fig. 3) along the Santa Venerina (VEN), Guzzi (GUZ) and SCA Faults with projected hypocentres of the 2002 Santa Venerina (red asterisk) and Scillichenti (yellow asterisk) earthquakes, the dashed black lines define the range of uncertainty; hypocentral depth from the Mt. Etna Seismic Catalogue 2000-2010 (Alparone et al., 2015); basement depth from Branca and Ferrara (2013).

Bayesian inversion of the 2022 aseismic creep event allowed us to conclude that the rupture is inside the volcanic pile, at about 300 m of depth. InSAR can only provide context for resolving the deformation onshore

because the satellites cannot record the deformation on the seafloor, so the rupture could actually be deeper. The continuity of the fault in the offshore sector is suggested by field evidence: along the coastline, the SCA Fault forms a discrete graben on the historical Mongibello lava flow and a vertical fault scarp due to rockfalls into the sea that have detached along the fault plane (Fig. 11c). Thus, assuming that the deformation continues offshore, we developed five profiles along the causative fault to assess the displacement changes (Figs. 11a and b). P1 shows the highest displacement as also observed in the field with 1,9 cm of East-West displacement (Fig. 9 and 11b), suggesting that it is the central sector of the modelled fault. P3 is in the northernmost area affected by the InSAR ground deformation and it is located about 400 m away from P1. Considering that P1 is about 150 m far from the coast, we infer that the deformation continues offshore. Therefore, the rupture is within the volcanic pile (Fig. 12) but the detachment depth could be underestimated, and it could hypothetically reach the top of the blue marly clay of the sedimentary basement, at ~600 m b.s.l. in the area according to Branca and Ferrara (2013). We assume that the blue marly clay can act as a detachment layer due to its weaker rheology as compared to the overlying volcanic rocks (*sensu* e.g., Borgia et al., 1992; Carveni and Bella, 1994; Carveni et al., 1997; Groppelli and Tibaldi, 1999; Apuani et al., 2013). This interpretation is compatible with what was observed for the 26 December 2018 earthquake along the Fiandaca Fault (FIA in Fig. 1a; Tringali et al., 2023).

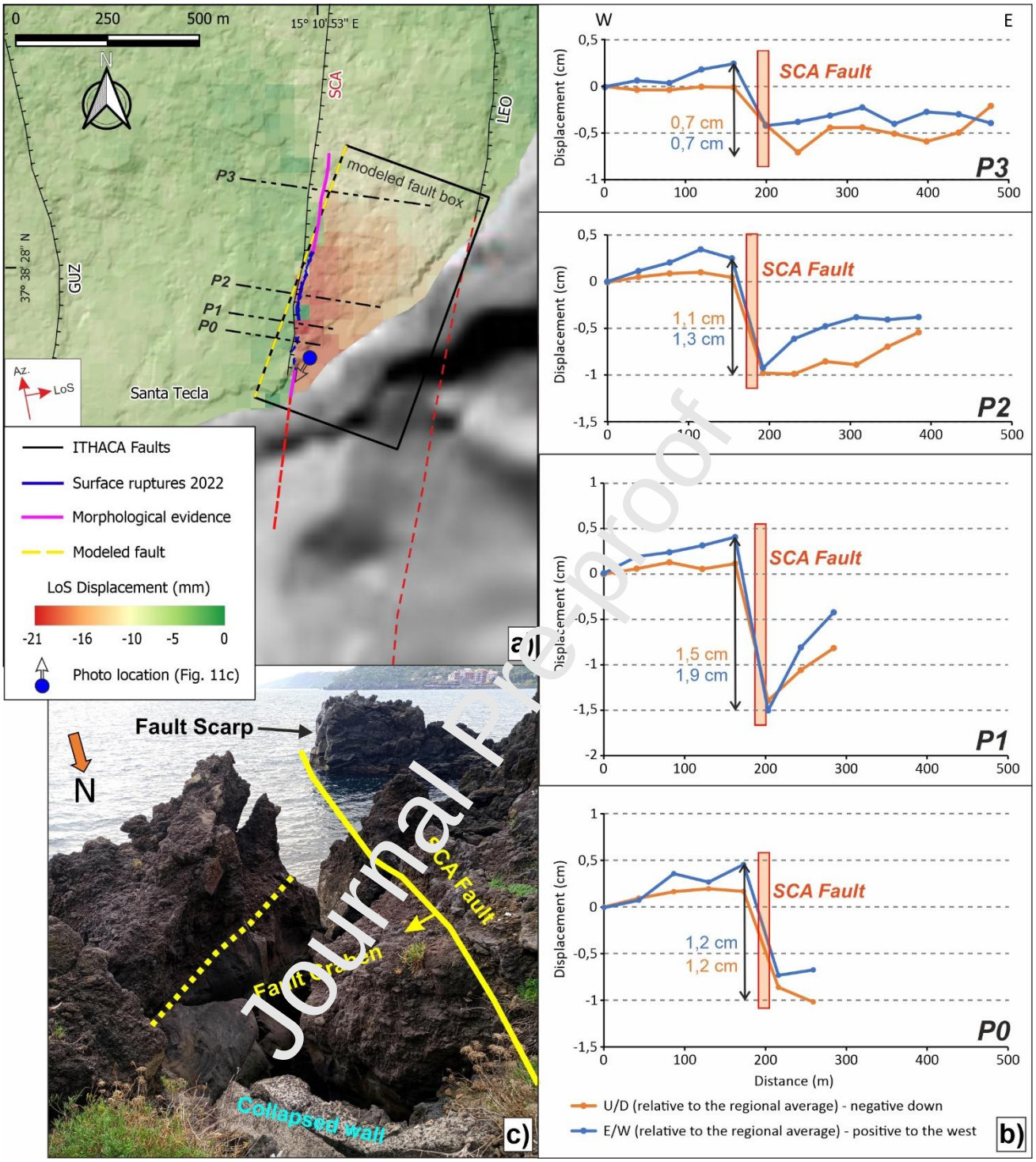

Figure 11: a) InSAR LOS displacement (ASC view) overprinted on a DTM (2 m resolution from Lidar flight ATA 2012-2013 of Regione Sicilia) with morphobathymetric features (Chiocci et al., 2011) and modelled deformation areas onshore and offshore, black lines are the ITHACA Faults (ITHACA Working Group, 2019), red dashed lines are the presumed faults prolongation offshore; b) Vertical (U/D) and East-West (E/W) displacement along 4 profiles, P1 shows the highest values indicating the central part of the modelled fault; c) Geomorphologic and tectonic features of the SCA Fault along the coastline.

Aseismic slip events are common where the depth of the blue marly clay is more shallow in the subsurface (Mattia et al., 2015; Palano et al., 2022; Tringali et al, 2023). In the Mt. Etna lower eastern flank, slow slip events can be influenced by fluid pressure, particularly by underground water circulation that affects rock strength and mechanical properties, causing ground movement at shallow depth (Mattia et al., 2015). The underground water table level in the southern portion of the SCA Fault is very shallow at less than 10 m,

which promotes aseismic creep phenomena even if the basement is at about 600 m b.s.l. Likewise, the San Leonardello Fault (LEO in Fig. 1a) has an aseismic behaviour in its S part for the same reason. In the epicenter area of the Scillichenti earthquake the volcanic pile thickness is ~600 m and the underground water level is ~90 m depth, possibly explaining the 2002 coseismic activation of the causative faults. In sum, 2002 flank instability and 2022 InSAR inversion suggests shallow faulting that accommodated Mt. Etna E flank gravitational sliding.

Concerning the geodynamic activity, the volcano had a year of frequent high-energy and short eruptions in the SE Crater that started on December 2020 and finished in December 2021, then was quiet in February 2022. The seismic activity was also very low with only 4 minor magnitude earthquakes recorded by the INGV-OE seismic network before the aseismic creep event in February 2022. The creep event was followed the day after by a short eruption in the SE Crater, with an intense explosive activity and the formation of a pyroclastic flow involving the summit area of the volcano. Therefore, February 2022 SCA aseismic creep could be a precursor of the eruptive activity that began at the SE crater and produced several eruptions until May-June 2022. Nevertheless, the data currently available are not sufficient to establish correlations between summit eruptions and aseismic creep events. However, it is possible to state that aseismic creep is also promoted by flank instability as observed in 2002 and 2018. It is clear that volcanic, tectonic and gravity processes are linked and strongly influence each other.

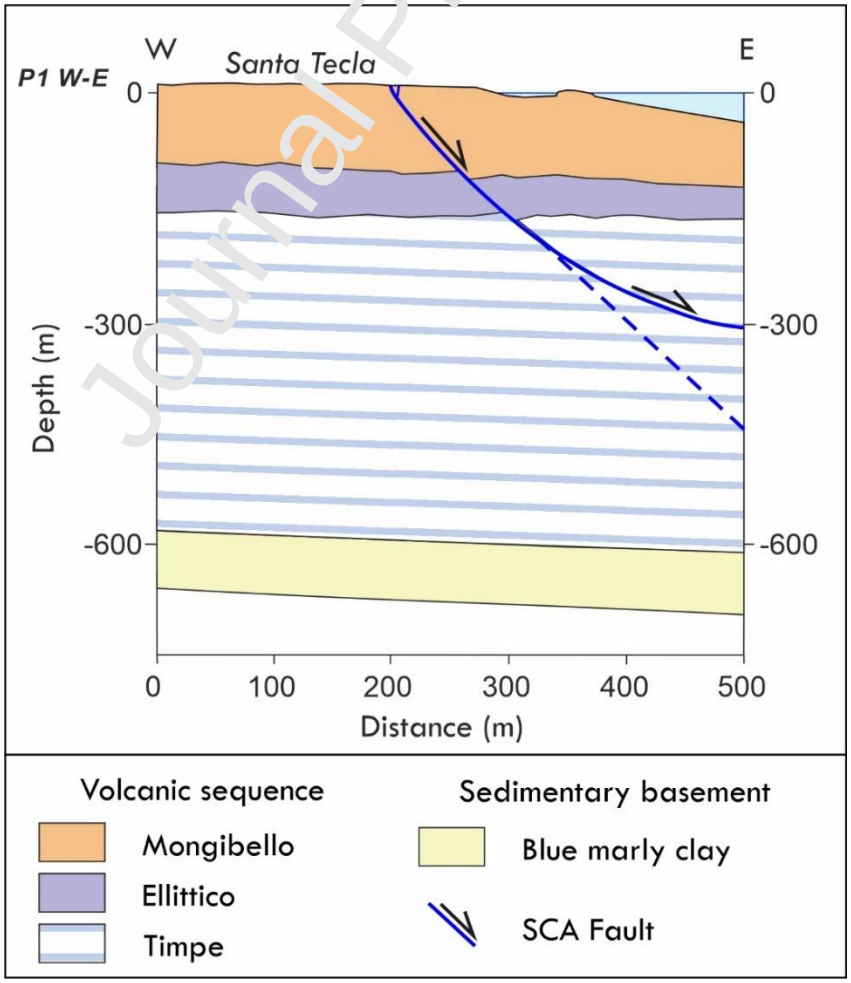

Figure 12: Conceptual geological cross section along P1 (see location in Figs. 9 and 11), the blue dashed line is the SCA Fault supposed continuation underground.

7. Conclusive remarks

Aseismic creep events and surface faulting are very common along the active faults of the Mt. Etna volcanic edifice. These can be analyzed from a multidisciplinary point of view, integrating observations from initial monitoring systems with seismic and geodetic networks, and satellite techniques. The surface faulting causes heavy damage to buildings and infrastructure, which significantly impacts the seismic hazard assessment in a densely populated area.

In this paper we presented new observations about the 29 October 2002 and 8 February 2022 surface faulting events, which occurred in the lower eastern flank of Mt. Etna and manifested in Santa Tecla as aseismic creep along the SCA Fault. Based on extensive field observations coupled with seismological data of the 2002 earthquakes, InSAR detected ground deformation and GBIS inversion, we have documented:

- SCA Fault showed 3 creep events with a recurrence time of about 20 years starting in the late 1970s.
- SCA Fault has a slip rate of 1.5 mm/y, considering its slip amount between 2002 and 2022 aseismic creep events.
- 2002 Santa Venerina and Scillichenti earthquakes ruptures were within the volcanic pile (Fig. 10).
- 2002 surface faulting propagation suggests a sliding of the E flank toward the SE as supported by the shallow seismicity, InSAR and geodetic data.
- SCA Fault has likely a prolongation offshore as suggested by field evidence and 2022 InSAR deformation pattern (Fig. 11); an offshore investigation could highlight the entire structure length.
- 2022 SCA Fault rupture was inside the volcanic pile (Fig. 12).
- SCA Fault accommodates the Mt. Etna E flank gravitational sliding, thus aseismic creep can be promoted by flank instability.
- Aseismic creep along the SCA Fault, and other faults close to the coastline, can be promoted by shallow water circulation.
- InSAR analyses are useful for detecting very small aseismic deformations that require verification by field surveys.

It is important to note that small events like the Santa Tecla 8 February 2022 aseismic creep could go unnoticed and remain scientifically undocumented. In this case, we only went to field-check after local residents provided specific information about ground breaks and other damages. Thus, further development of monitoring and investigation techniques and local citizen interviews might allow us to document similar events in the future so that we can better understand the complex volcano-tectonics of Mt. Etna volcano. Understanding these phenomena at different spatiotemporal scales is valuable for improving our knowledge of the surface faulting and volcanic hazard assessments for mitigating the risk of vulnerable population centers.

Author contributions

Giorgio Tringali: Conceptualization, Investigation, Methodology, Formal analysis, Data Curation, Writing - Original Draft, Writing - Review & Editing, Visualization. **Domenico Bella:** Investigation, Formal analysis, Writing - Review & Editing, Visualization. **Franz Livio:** Methodology, Software, Formal analysis, Data Curation, Writing - Review & Editing, Visualization. **Maria Francesca Ferrario:** Writing - Review & Editing, Visualization. **Gianluca Groppelli:** Writing - Review & Editing, Visualization. **Rosario Pettinato:** Investigation, Visualization. **Alessandro Maria Michetti:** Writing - Review & Editing, Visualization, Supervision.

Data availability

Seismological data were retrieved from the INGV websites at http://cnt.rm.ingv.it/event/21285011 and http://sismoweb.ct.ingv.it/Etna/catalogs/EtnaRCSC/. In particular the Mt. Etna Seismic Catalog 2000-2010 is available at http://sismoweb.ct.ingv.it/Etna/catalogs/2000_2010/. The ITHACA database of capable fault is publicly available at http://sgi2.isprambiente.it/ithacaweb/viewer/ The CPTI15 4.0 version of the Parametric Catalogue of Italian Earthquakes is available at https://emidius.mi.ingv.it/CPTI15-DBMI15/description_CPTI15_en.htm.

The data of the ground ruptures as shapefile format are available on the Zenodo repository (https://doi.org/10.5281/zenodo.7263296).

The electronic supplement to this article includes the details of the InSAR inversion preformed with GBIS and detailed maps of the 2002 coseismic surface ruptures.

Declaration of competing interest

The authors declare that they have no known competing financial interests or personal relationships that could have appeared to influence the work reported in this paper.

Acknowledgments

We are deeply grateful with the local people in Santa Tecla, Santa Venerina, San Giovanni Bosco, Scillichenti and nearby areas who allowed us to enter into their properties and informed us about the formation of the surface ruptures observed in their land and homes. We are grateful to the INGV-OE seismic network staff who ensure the regular working of seismic stations and to the "Gruppo Analisi Dati Sismici" for earthquake data. We thank the editor and anonymous reviewers for their comments and suggestions that improved the final version of this manuscript. We thank M. Neri for critical discussions about the depth of detachments and K. Nicoll for the careful English text revision. G. Tringali research activity has been supported by the Università degli Studi dell'Insubria grant.

References

Acocella, V., Behncke, B., Neri, M., and D'Amico, S. (2003), Link between major flank slip and 2002–2003 eruption at Mt. Etna (Italy), Geophys. Res. Lett., 30, 2286, doi:10.1029/2003GL018642, 24.

Alparone, S. C., Maiolino, V., Mostaccio, A., Scaltrito, A., Ursino, A., Barberi, G., et al. (2015). Mt. Etna

Seismic Catalog 2000-2010 [Data set]. Istituto Nazionale di Geofisica e Vulcanologia (INGV) - Osservatorio Etneo. https://doi.org/10.13127/etnasc/2000_2010

Alparone, S, Barberi, G, Giampiccolo, E, et al., 2020. Seismological constraints on the 2018 Mt. Etna (Italy) flank eruption and implications for the flank dynamics of the volcano. Terra Nova. 2020; 32:334–344. https://doi.org/10.1111/ter.12463

Apuani, T., Corazzato, C., Merri, A. & Tibaldi, A., 2013. Understanding Etna flank instability through numerical models. Journal of volcanology and geothermal research 251, 112–126

Azzaro, R., 1999. Earthquake surface faulting at Mount Etna volcano (Sicily) and implications for active tectonics. Journal of Geodynamics 28, 193–213.

Azzaro, R., Branca, S., Gwinner, K, Coltelli, M., 2012. The volcano-tectonic map of Etna volcano, 1:100.000 scale: an integrated approach based on a morphotectonic analysis from high-resolution DEM constrained by geologic, active faulting and seismotectonic data. Italian Journal of Geosciences. 2012; 131 (1): 153–170. doi: https://doi.org/10.3301/IJG.2011.29

Azzaro, R., Bonforte, A., Branca, S. & Guglielmino, F., 2013. Geometry and kinematics of the fault systems controlling the unstable flank of Etna volcano (Sicily). Journal of Volcanology and Geothermal Research 251, 5–15.

Azzaro, R, Bonforte, S. D'Amico, Guglielmino, F., Scarfì, L., 2020. Stick-slip vs. stable sliding fault behaviour: A case-study using a multidisciplinary approach in the volcanic region of Mt. Etna (Italy). Tectonophysics, 790, 228554, https://doi.org/10.1016/j.tecto.2020.228554.554

Bagnardi, M., Hooper, A., 2018. Inversion of surface deformation data for rapid estimates of source parameters and uncertainties: A Bayesian approach. Geochemistry, Geophysics, Geosystems 19, 2194– 2211.

Barberi, G., Cocina, O., Maiolino, V., Musumeci, C., and Privitera, E., 2004. Insight into Mt. Etna (Italy) kinematics during the 2002–2003 eruption as inferred from seismic stress and strain tensors, Geophys. Res. Lett., 31, L21614, doi:10.1029/2004GL020918.

Blumetti, A. M., Di Manna, P., Ferreli, L., Fiorenza, D. & Vittori, E. 2007. Reduction of environmental risk from capable faults: the case of the Eastern Etna region (eastern Sicily, Italy). Quaternary International 173, 45–56.

Bonaccorso, A., Bonforte, A., Guglielmino, F., Palano, M. and Puglisi, G., 2006. Composite ground deformation pattern forerunning the 2004–2005 Mount Etna eruption, J. Geophys. Res., 111, B12207, doi:10.1029/2005JB004206.

Bonforte, A., Guglielmino, F. & Puglisi, G., 2019. Large dyke intrusion and small eruption: The December 24, 2018 Mt. Etna eruption imaged by Sentinel-1 data. Terra Nova 31, 405–412. Alparone et al., 2020

Bonforte, A., Guglielmino, F., Coltelli, M., Ferretti, A. & Puglisi, G., 2011. Structural assessment of Mount Etna volcano from Permanent Scatterers analysis. Geochemistry, Geophysics, Geosystems 12.

Borgia, A., Ferrari, L. & Pasquarè, G., 1992. Importance of gravitational spreading in the tectonic and volcanic evolution of Mount Etna. Nature 357, 231–235. Carveni and Bella, 1994;

Branca, S. & Ferrara, V., 2013 The morphostructural setting of Mount Etna sedimentary basement (Italy): Implications for the geometry and volume of the volcano and its flank instability. Tectonophysics 586, 46– 64.

Branca, S., Coltelli, M., Groppelli, G. & Lentini, F., 2011 Geological map of Etna volcano, 1: 50,000 scale. Italian Journal of Geosciences 130, 265–291.

Carveni, P. & Bella, D., 1994. Aspetti geomorfologici legati ad attività sismica su vulcani attivi: il basso versante orientale dell'Etna come modello di studio. Boll. Acc. Gioenia Sc. Nat. 27, 253–285.

Carveni, P., Filetti, G. & Bella, D., 1997. Aspetti geomorfologici e sismologici connessia a fenomeni di tettonica gravitativa nel basso versante orientale dell'Etna. Geografia fisica e dinamica quaternaria 20, 43– 49.

Chiocci, F. L., Coltelli, M., Bosman, A. & Cavallaro, D., 2011. Continental margin large-scale instability controlling the flank sliding of Etna volcano. Earth and Planetary Science Letters 305, 57–64 (2011).

Doglioni, C., Innocenti, F., & Mariotti, G., 2001. Why Mt Etna? Terra Nova 13, 25–31 (2001).

Groppelli, G. & Norini, G., 2011. Geology and tectonics of the southwestern boundary of the unstable sector of Mt. Etna (Italy). Journal of volcanology and geothermal research 208, 66–75.

Gross, F. et al., 2016. The limits of seaward spreading and slope instability at the continental margin offshore Mt Etna, imaged by high-resolution 2D seismic data. Tectonophysics 667, 63–76.

Grünthal, G., 1998. European Macroseismic Scale 1998 (EMS-98). European Seismological Commission, sub commission on Engineering Seismology, Working Group Macroseismic Scales. Conseil de l'Europe, Cahiers du Centre Européen de Géodynamique et de Séismologie, Vol. 15, Luxembourg.

ITHACA Working Group, 2019. ITHACA (ITaly HAzard from CApable faulting), A database of active capable faults of the Italian territory. Version December 2019; ISPRA Geological Survey of Italy. Web Portal http://sgi2.isprambiente.it/ithacaweb/Mappatura.aspx.

Mancini, F., Grassi, F., Cenni, N., 2021. A Workflow Based on SNAP–StaMPS Open-Source Tools and GNSS Data for PSI-Based Ground Deformation Using Dual-Orbit Sentinel-1 Data: Accuracy Assessment with Error Propagation Analysis. Remote Sensing 13, 753. https://doi.org/10.3390/rs13040753.

Mattia, M. et al., 2015. A comprehensive interpretative model of slow slip events on Mt. Etna's eastern flank. Geochemistry, Geophysics, Geosystems 16, 635–658

Mattia, M., Bruno, V., Montgomery-Brown, E., Patanè, D., Barberi, G., & Coltelli, M., 2020. Combined seismic and geodetic analysis before, during and after the 2018 Mount Etna eruption. Geochemistry, Geophysics, Geosystems, 21, e2020GC009218. https://doi.org/10.1029/2020GC009218.

Monaco, C. et al., 2005. Tectonic control on the eruptive dynamics at Mt. Etna Volcano (Sicily) during the 2001 and 2002–2003 eruptions. Journal of Volcanology and Geothermal Research 144, 211–233.

Neri, M., Acocella, V., Behncke, B., 2004. The role of the Pernicana Fault System in the spreading of Mt. Etna (Italy) during the 2002–2003 eruption. Bull. Volcanol. 66, 417–430. https://doi.org/10.1007/s00445- 003-0322-x.

Neri, M., Casu, F., Acocella, V., Solaro, G., Pepe, S., Berardino, P., Sansosti, E., Caltabiano, T., Lundgren, P., and Lanari, R., 2009. Deformation and eruptions at Mt. Etna (Italy): A lesson from 15 years of observations, Geophys. Res. Lett., 36, L02309, https://doi.org/0.1029/2008GL036151.

Neri, M., Guglielmino, F., & Rust, D., 2007. Flank instability on Mount Etna: Radon, radar interferometry, and geodetic data from the southwestern boundary of the unstable sector. Journal of Geophysical Research: Solid Earth 112.

Norini, G., & Acocella, V., 2011. Analogue modeling of flank instability at Mount Etna: Understanding the driving factors. Journal of Geophysical Research: Solid Earth 116.

Okada, Y., 1985. Surface deformation due to shear and tensile faults in a half-space. Bulletin of the Seismological Society of America 75, 1135–1154.

Palano, M., Sparacino, F., Gambino, P., D'Agostino, N., Calcaterra, S., 2022. Slow slip events and flank instability at Mt. Etna volcano (Italy), Tectonophysics, Volume 836, 2022, 229414, ISSN 0040-1951, https://doi.org/10.1016/j.tecto.2022.229414.

Puglisi, G., Bonforte, A., Ferretti, A., Guglielmino, F., Palano, M., and Prati, C., 2008. Dynamics of Mount Etna before, during, and after the July–August 2001 eruption inferred from GPS and differential synthetic aperture radar interferometry data. J. Geophys. Res. Solid Earth 113, B06405. doi:10.1029/2006jb004811.

Rasà, R., Azzaro, R., & Leonardi, O., 1996. Aseismic creep on faults and flank instability at Mount Etna volcano, Sicily. Geological Society, London, Special Publications 110, 179–192.

Riccò, A., 1909. Il terremoto di San Giovanni Bosco. Boll. Acc. Gioenia, fasc.10, dicembre 1909.

Ruch, J. et al., 2012. How do volcanic rift zones relate to flank instability? Evidence from collapsing rifts at Etna. Geophysical Research Letters 39.

Rust, D., Behncke, B. Neri, M. and Ciocanel, A., 2005. Nested zones of instability in the Mount Etna volcanic edifice, Sicily. Jour. Volcanology and Geothermal Research, Special Issue on the Tectonics and Physics of Volcanoes, 144, 137-153. doi:10.1016/j.jvolgeores.2004.11.021

Scarfì, L, Messina, A., Cassisi, C., 2013. Sicily and southern Calabria focal mechanism database: a valuable tool for local and regional stress-field determination. Ann. Geophys. Doi: https://doi.org/10.4401/ag-6109.

Silvestri, O., (1879a): La doppia eruzione e i terremoti dell'Etna nel 1879. Boll. R. Com. Geol. It., 11-12, novembre-dicembre, 590-604.

Silvestri, O., 1879. Fenomeni dell'Etna successivi all'ultima eruzione. Bullettino del Vulcanismo Italiano, anno VI, (8-11, agosto-novembre), 119-124

Siniscalchi, A., S., Tripaldi, M., Neri, Balasco, M., Romano, G., Ruch, J., and Schiavone D., 2012. Flank instability structure of Mt. Etna inferred by a magnetotelluric survey,J. Geophys. Res.,117, B03216, doi:10.1029/2011JB008657.

Solaro, G. et al., 2010. Anatomy of an unstable volcano from InSAR: Multiple processes affecting flank instability at Mt. Etna, 1994–2008. Journal of Geophysical Research: Solid Earth 115.

Tibaldi, A. & Groppelli, G., 2002. Volcano-tectonic activity along structures of the unstable NE flank of Mt. Etna (Italy) and their possible origin. Journal of Volcanology and Geothermal Research 115, 277–302.

Tringali, G., Bella, D., Livio, F.A., Ferrario, M.F., Groppelli, G., Blumetti, A.M., Di Manna, P., Vittori, E., Guerrieri, L., Porfido, S., Boso, D., Pettinato, R., Paradiso, G., & Michetti, A.M., 2023. Fault rupture and aseismic creep accompanying the December 26, 2018, Mw 4.9 Fleri earthquake (Mt. Etna, Italy): Factors affecting the surface faulting in a volcano-tectonic environment. Quat. Int. 651, 25–41. https://doi.org/10.1016/j.quaint.2021.12.019.

Tringali, G., & Bella, D., 2022. 2002 and 2022 fault ruptures along the Timpe faults system (Mt. Etna) [Data set]. Zenodo. https://doi.org/10.5281/zenodo.7263297

Urlaub, M., Geersen, J., Petersen, F., Gross, F., Bonforte, A., Krastel, S., and Kopp, H., 2022. The Submarine Boundaries of Mount Etna's Unstable Southeastern Flank. Front. Earth Sci.

10:810790. doi: 0.3389/feart.2022.810790.

Urlaub, M. et al., 2018. Gravitational collapse of Mount Etna's southeastern flank. Science Advances 4, eaat9700.

Walter, T. R., Acocella, V., Neri, M. & Amelung, F., 2005. Feedback processes between magmatic events and flank movement at Mount Etna (Italy) during the 2002–2003 eruption. Journal of Geophysical Research: Solid Earth 110.

Aseismic creep and gravitational sliding on the lower eastern flank of Mt. Etna: insights from the 2002 and 2022 fault rupture events between Santa Venerina and Santa Tecla

Giorgio Tringali [a]*, Domenico Bella [b], Franz Livio [a], Maria Francesca Ferrario [a], Gianluca Groppelli [c], Rosario Pettinato [b] & Alessandro Maria Michetti [a-d]

Author affiliations:

e) Università degli Studi dell'Insubria, Dipartimento di Scienza ed Alta Tecnologia, Via Valleggio 11, 22100 Como (CO), Italy

f) Studio di Geologia Domenico Bella, Via N. Martoglio 13, 95024 Acireale (CT), Italy

g) CNR – Consiglio Nazionale delle Ricerche, Istituto di Geologia Ambientale e Geoingegneria, Milano (MI), Italy

h) INGV – Istituto Nazionale di Geofisica e Vulcanologia, Osservatorio Vesuviano, via Diocleziano 328, 80124, Napoli (NA), Italy

**Corresponding author:* gtringali@uninsubria.it

Keywords: Etna, aseismic creep, earthquake, surface faulting, volcano-tectonic deformation

Abstract

Fault creep along the lower eastern flank of Mt. Etna volcano has been documented since the end of the 19th century and significantly contributes to the surface faulting hazard in the area. On 29 October 2002, during a seismic swarm related to dyke intrusions, two earthquakes caused extensive damage and surface faulting in an area between the Santa Venerina and Santa Tecla villages. On the same day after the two earthquakes, an episodic aseismic creep occurred along the Scalo Pennisi Fault close to the Santa Tecla coastline. On 8 February 2022, during another aseismic creep event along the Scalo Pennisi Fault, we observed the reopening of the pre-existing 2002 ground ruptures mostly as pure dilational fractures. We mapped the 2002 and 2022 surface ruptures, and collected data on displacement, length, and pattern of ground breaks. Ground ruptures affected structures located along the activated fault segments, including roads, walls and buildings. The 2002 surface faulting propagation can be ascribed to a sliding of the Mt. Etna eastern flank toward the SE, as also suggested by the related shallow seismicity, and InSAR and geodetic data between 2002 and 2005. For the 2022 event, differential InSAR data, acquired in both descending and ascending views, allowed us to decompose Line of Sight (LOS) displacement into horizontal and vertical components. We detect a ~700 long and ~500 m wide deformation zone with a downward and eastward motion (max displacement ~1,5 cm) consistent with a normal fault. We inverted the InSAR– detected surface deformation using a uniform-slip fault model and obtained a shallow detachment for the causative fault, located at ~300 m depth, within the volcanic pile. This is the first in-depth study along the Scalo Pennisi Fault to suggest a shallow faulting that accommodates Mt. Etna E flank gravitational sliding.

Giorgio Tringali: Conceptualization, Investigation, Methodology, Formal analysis, Data Curation, Writing - Original Draft, Writing - Review & Editing, Visualization. **Domenico Bella:** Investigation, Formal analysis, Writing - Review & Editing, Visualization. **Franz Livio:** Methodology, Software, Formal analysis, Data Curation, Writing - Review & Editing, Visualization. **Maria Francesca Ferrario:** Writing - Review & Editing, Visualization. **Gianluca Groppelli:** Writing - Review & Editing, Visualization. **Rosario Pettinato:** Investigation, Visualization. **Alessandro Maria Michetti:** Writing - Review & Editing, Visualization, Supervision.

Declaration of interests

☒The authors declare that they have no known competing financial interests or personal relationships that could have appeared to influence the work reported in this paper.

☐The authors declare the following financial interests/personal relationships which may be considered as potential competing interests:

Tringali et al. 2023

Highlights

- We mapped 2002 and 2022 Mt. Etna eastern flank surface faulting.
- 2002 strongest earthquakes were within the volcanic pile and the surface faulting propagation, InSAR and geodetic data suggest a gravitational sliding of the eastern flank toward the SE.
- InSAR surface deformation analysis and inversion for 2022 Scalo Pennisi Fault aseismic creep show a rupture inside the volcanic pile.
- We suggest shallow faulting for the Scalo Pennisi Fault which accommodates Etna eastern flank gravitational sliding with a possible detachment on top of the sedimentary basement.